



## Magnetothermoelectric properties of $\text{Bi}_2\text{Se}_3$

Benoît Fauqué,<sup>1,\*</sup> Nicholas P. Butch,<sup>2,†</sup> Paul Syers,<sup>2</sup> Johnpierre Paglione,<sup>2</sup> Steffen Wiedmann,<sup>3</sup>  
Aurélié Collaudin,<sup>1</sup> Benjamin Grena,<sup>1,4</sup> Uli Zeitler,<sup>3</sup> and Kamran Behnia<sup>1</sup>

<sup>1</sup>*LPEM (UPMC-CNRS), Ecole Supérieure de Physique et de Chimie Industrielles, F-75005 Paris, France*

<sup>2</sup>*Center for Nanophysics and Advanced Materials, Department of Physics, University of Maryland, College Park, Maryland 20742, USA*

<sup>3</sup>*High Field Magnet Laboratory, Institute for Molecules and Materials, Radboud University Nijmegen, Toernooiveld 7,  
NL-6525 ED Nijmegen, The Netherlands*

<sup>4</sup>*Department of Physics, Ecole Polytechnique, Palaiseau 91120, France*

(Received 7 September 2012; revised manuscript received 12 December 2012; published 25 January 2013)

We present a study of entropy transport in  $\text{Bi}_2\text{Se}_3$  at low temperatures and high magnetic fields. In the zero-temperature limit, the magnitude of the Seebeck coefficient quantitatively tracks the Fermi temperature of the three-dimensional Fermi surface at the  $\Gamma$  point as the carrier concentration changes by two orders of magnitude ( $10^{17}$  to  $10^{19}$   $\text{cm}^{-3}$ ). In high magnetic fields, the Nernst response displays giant quantum oscillations indicating that this feature is not exclusive to compensated semimetals. A comprehensive analysis of the Landau level spectrum firmly establishes a large  $g$  factor in this material and a substantial decrease of the Fermi energy with increasing magnetic field across the quantum limit. Thus, the presence of bulk carriers significantly affects the spectrum of the intensively debated surface states in  $\text{Bi}_2\text{Se}_3$  and related materials.

DOI: [10.1103/PhysRevB.87.035133](https://doi.org/10.1103/PhysRevB.87.035133)

PACS number(s): 72.15.Jf

### I. INTRODUCTION

The  $\text{Bi}_2\text{X}_3$  family ( $\text{X} = \text{Se}, \text{Te}$ ) is attracting tremendous attention as a topological insulator (TI). Recently, the existence of this class of bulk insulators was predicted and confirmed.<sup>1</sup> In a TI, the bulk energy gap is traversed by spin polarized surface states. Therefore, the electrical conduction is expected to occur only at the surface. In practice, however, these materials are often low-density bulk metals. Interestingly, many of the TI of the first and the second generation are well-known thermoelectric materials<sup>2</sup> and present a sizable thermoelectric figure of merit. This quantity,  $ZT = \frac{S^2 T}{\kappa \rho}$  (here  $S$  is the Seebeck coefficient,  $\kappa$  is thermal conductivity, and  $\rho$  is resistivity) characterizes the thermoelectric efficiency of a material. To this date, the largest thermoelectric figure of merit in a bulk material at room temperature has been reported in  $\text{Bi}_2\text{Te}_3$  ( $ZT = 0.8$  at  $T = 300$  K<sup>3,4</sup>).

In spite of the fundamental and technological interest in  $\text{Bi}_2\text{Se}_3$  and  $\text{Bi}_2\text{Te}_3$ , their thermoelectric response has not been investigated at temperatures low enough to distinguish between the two competing (semiconducting vs metallic) ground states. In this paper, we report on measurements of Seebeck and Nernst effect in  $n$ -type  $\text{Bi}_2\text{Se}_3$  with a bulk carrier concentration varying from  $10^{19}$   $\text{cm}^{-3}$  to  $10^{17}$   $\text{cm}^{-3}$  at low temperature and in a magnetic field as strong as 32 T. We find that the low-temperature magnitude of the Seebeck coefficient is set by the Fermi temperature, which can be directly extracted from the measured properties of the metallic Fermi surface. The transverse thermoelectric (Nernst) response displays large quantum oscillations. Such oscillations were previously reported in low-density compensated semimetals, bismuth and graphite. Their observation in a single-band uncompensated system indicates that they are generic to any low-carrier system pushed to the quantum limit by a sufficiently strong magnetic field. Analysis of quantum oscillations allows us to (i) document a continuous field-induced shift in chemical potential affecting the periodicity of the oscillations;

(ii) quantify the magnitude of Zeeman splitting in this system, which is expected to host a large spin-orbit coupling. These two points are crucial in discussing the Landau spectrum of bulk states. They also affect the analysis of the Landau spectrum of the surface carriers, which share the same chemical potential with bulk.

### II. QUANTUM OSCILLATIONS IN SEEBECK AND NERNST EFFECT

Measurements of longitudinal ( $S = \frac{E_x}{\Delta_x T}$ ) and the transverse ( $N = \frac{E_y}{|\Delta_x T|}$ ) thermoelectric response were performed on a standard one-heater-two-thermometers setup. For all samples, the electric current and the thermal gradient were applied in the plane of the quintuple layers and the magnetic field was oriented along the trigonal direction (perpendicular to the layers). The samples used in this study are similar to those previously studied by longitudinal and transverse magnetoresistance experiments<sup>5</sup> and described there.

In Fig. 1, we compare the electrical transport and the entropy transport in two samples  $A_1$  and  $B_1$  with typical bulk concentrations of  $10^{19}$   $\text{cm}^{-3}$  to  $10^{17}$   $\text{cm}^{-3}$ . For both samples,  $\rho_{xx}$  and  $\rho_{yx}$  display quantum oscillations on top of an almost linear monotonic base as previously reported and discussed.<sup>5-8</sup> In the presence of a field of about 10 T, we find for the two concentrations that  $\rho_{xx} \approx \rho_{yx}$  whereas  $S \gg N$  (the typical ratios are 100 for  $A_1$  and 10 for  $B_1$ ). As in the case of the electrical transport,  $S$  and  $N$  display quantum oscillations with a phase shift of  $\frac{\pi}{2}$ . The oscillations are particularly pronounced in  $N$  (in the case of  $A_1$  they dominate the signal). The surprising sensitivity of the Nernst effect to quantum oscillations in  $\text{Bi}_2\text{Se}_3$  is indeed reminiscent of those reported in bismuth<sup>9</sup> and graphite.<sup>10</sup> The origin of these giant quantum oscillations is the subject of ongoing theoretical research.<sup>11-13</sup> These two elemental semimetals are, however, compensated systems, whereas the (bulk) Fermi surface of  $\text{Bi}_2\text{Se}_3$ , as we will see below is a single band at the  $\Gamma$  point. Therefore, the observation

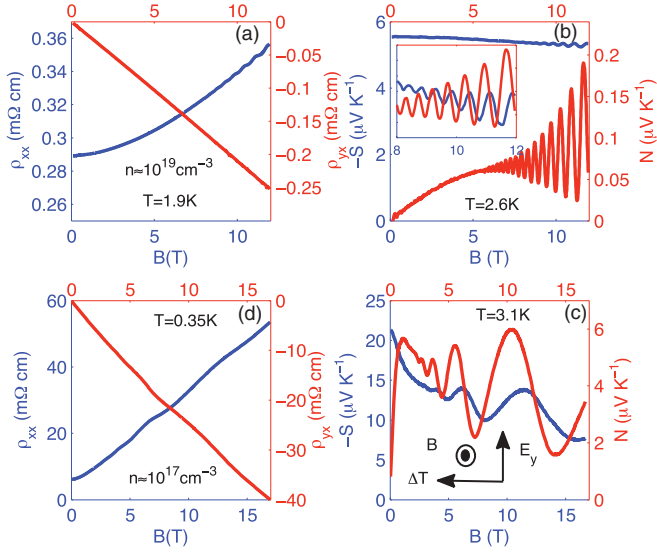


FIG. 1. (Color online) Electrical and entropy transport measurements of  $\text{Bi}_2\text{Se}_3$  for the samples  $A_1$  [ $n(A_1) \approx 1e19 \text{ cm}^{-3}$ ] and  $B_1$  [ $n(B_1) \approx 1e17 \text{ cm}^{-3}$ ] (a)  $\rho_{xx}$  (in blue) and  $\rho_{yx}$  (in red) of  $A_1$  as a function of the magnetic field for  $T = 1.9 \text{ K}$ . (b)  $S$  (in blue) and  $N$  (in red) of  $A_1$  as a function of the magnetic field for  $T = 2.6 \text{ K}$  (the insert shows a zoom of  $S$  and  $N$  between 8 and 12 T). (c)  $\rho_{xx}$  (in blue) and  $\rho_{yx}$  (in red) of  $B_1$  as a function of the magnetic field for  $T = 350 \text{ mK}$ . (d)  $S$  (in blue) and  $N$  (in red) of  $B_1$  as a function of the magnetic field for  $T = 3.1 \text{ K}$ .

reported here establishes that this effect is not exclusive to compensated systems. We note that there are several reports on Nernst quantum oscillations with a large amplitude and a small frequency in metals like zinc<sup>14</sup> and aluminum<sup>15</sup> or in doped semiconductors such as  $n$ -type InAs<sup>16</sup> and iron-doped HgSe.<sup>17</sup>

### A. Effective masse and Dingle temperature

Next, we focus our attention on the temperature dependence of the quantum oscillations in the thermoelectric properties, which have been so far poorly studied. In Fig. 2,  $\frac{\nu}{T} = \frac{N}{TB}$  is plotted as a function of  $B^{-1}$  for various temperature. In both cases, the signal is periodic in  $B^{-1}$ . The difference of the period between the two samples simply reflects the difference in the carrier concentrations. In both cases, the oscillations disappear at a typical temperature of 20 K suggesting rather similar low effective mass for both concentrations. Following the standard Lifshitz-Kosevich theory,<sup>18</sup> we fit the temperature dependence of the oscillating part of  $\frac{\nu}{T}$  to:  $RT = \frac{X}{\sinh(X)}$  where  $X = \frac{14.69m^*T}{B}$ . The data and the fit are shown in Fig. 2(c). We found, respectively,  $m^*(A_1)/m_0 = 0.20 \pm 0.03$  and  $m^*(B_2)/m_0 = 0.18 \pm 0.03$  in good agreement with the cyclotron mass deduced by Shubnikov-de Haas oscillations.<sup>5,7,8</sup>

By studying the field dependence, we can also extract additional information such as a Dingle temperature. In Fig. 3, we report the so-called ‘‘Dingle plot’’ for four temperatures:  $T = 2.8 \text{ K}$ ,  $8.3 \text{ K}$ ,  $12.5 \text{ K}$ , and  $15.8 \text{ K}$  for the sample  $A_1$ . In the context of the Lifshitz-Kosevich formalism,<sup>18</sup> we expect that

$$\ln\left(\frac{A}{RT}\right) = -\alpha T_D m^* \times \frac{1}{B}. \quad (1)$$

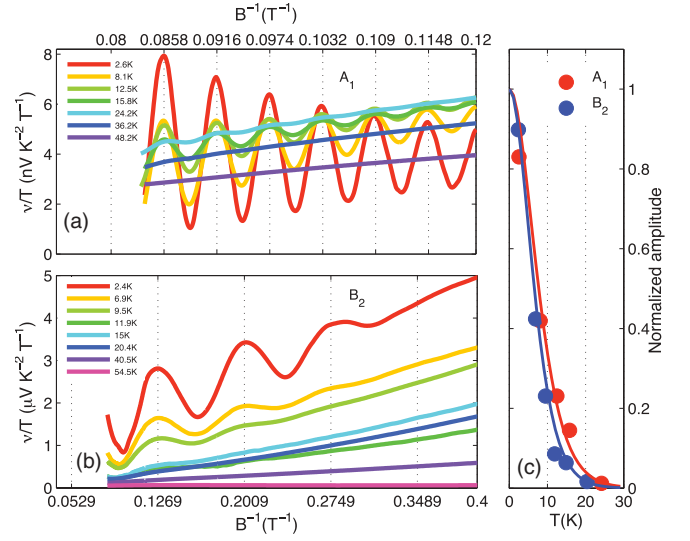


FIG. 2. (Color online) (a) and (b)  $\frac{\nu}{T} = \frac{N}{TB}$  as a function of  $B^{-1}$  for the sample  $A_1$  and  $B_2$  (sample different of  $B_1$  with a similar bulk concentration) for the various temperatures explored. (c) Temperature dependence of the amplitude of the oscillations of the sample  $A_1$  (in red) and  $B_2$  (in blue). The line corresponds to a fit using the Lifshitz-Kosevich formula (see the text).

For the four temperatures, the field dependence of  $\ln(\frac{A}{RT})$  is linear. From Eq. (1), we found a Dingle temperature  $T_D = 10 \pm 1 \text{ K}$  in good agreement with Shubnikov-de Haas measurements.<sup>5-8</sup> The remarkable simplicity of our analysis of the quantum oscillations  $\frac{\nu}{T}$  is related to the absence of a phonon drag contribution in the transverse thermoelectric response (contrary to its significant contribution in the Seebeck effect). This point is consistent with the early analysis of Tiede *et al.*<sup>17</sup> in the case of iron-doped HgSe.

### B. Magnitude of the Seebeck and Nernst effect

The magnitude of the thermoelectric response is dramatically affected by the change in the carrier concentration. Figures 4(a) and 4(b) present  $\frac{S}{T}$  and  $\frac{\nu}{T}$  as a function of temperature for the four samples studied. As the doping passes

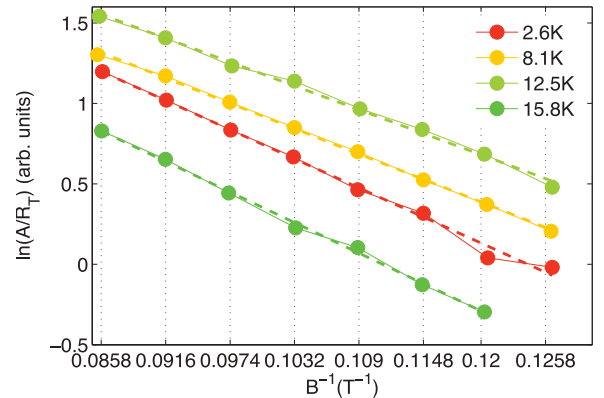


FIG. 3. (Color online) ‘‘Dingle plot’’  $\ln(\frac{A}{RT})$  as a function of  $B^{-1}$ . A corresponds to the amplitude of the oscillations as observed in  $\frac{\nu}{T}$  and  $RT = \frac{X}{\sinh(X)}$  where  $X = \frac{14.69m^*T}{B}$  ( $m^* = 0.2m_0$  in the case of  $A_1$ ).

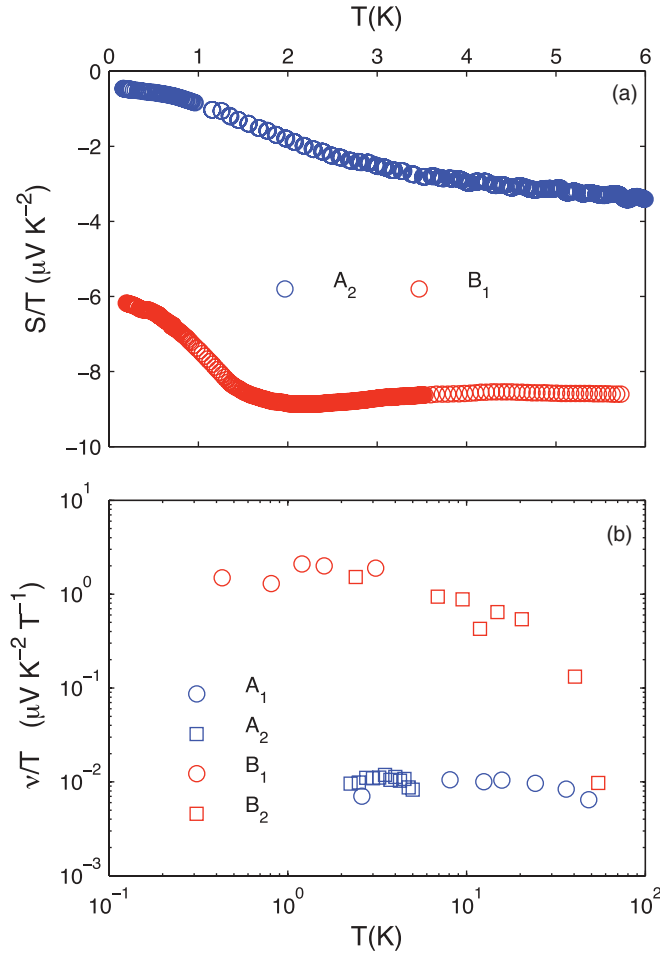


FIG. 4. (Color online) (a)  $\frac{S}{T}$  as a function of the temperature for A<sub>2</sub> (same batch as A<sub>1</sub> with a slightly lower concentration) and B<sub>1</sub>. (b)  $\frac{\nu}{T}$  at  $B = 1$  T as a function of the temperature for A<sub>1</sub>, A<sub>2</sub>, B<sub>1</sub>, and B<sub>2</sub>.

from  $10^{19} \text{ cm}^{-3}$  to  $10^{17} \text{ cm}^{-3}$ ,  $\frac{S}{T}$  increases by one order of magnitude and  $\frac{\nu}{T}$  increases by two orders of magnitude. In the Fermi liquid picture for a one-band system, the diffusive Seebeck is expected to be  $T$  linear in the zero-temperature limit with a magnitude proportional to  $1/T_F$ :

$$\frac{S}{T} = -\frac{\pi^2}{2} \frac{k_B}{e} \frac{1}{T_F}. \quad (2)$$

Similarly the solution of the Boltzmann equation for the Nernst response leads to  $\frac{\nu}{T} = -\frac{\pi^2}{3} \frac{k_B^2 T}{m^*} \frac{\partial \tau}{\partial \epsilon} |_{\epsilon=\epsilon_F}$  which can be simplified and rewritten as<sup>19</sup>

$$\frac{\nu}{T} \approx 283 \frac{\mu}{T_F} [\mu\text{V K}^{-2} \text{T}^{-1}]. \quad (3)$$

Empirically, these simple equations give a rough account of the magnitude of transport coefficients across several orders of magnitude.<sup>19,20</sup>

Bi<sub>2</sub>Se<sub>3</sub> provides a particularly compelling opportunity to check the robustness of Eqs. (2) and (3) in a wide window of carrier concentration with a barely changing Fermi surface topology. The mobility and the Fermi energy can both be extracted from the data on quantum oscillations. Table I lists the values of  $\frac{S}{T}$  and  $\frac{\nu}{T}$  obtained at the lowest temperature

TABLE I. Properties of Bi<sub>2</sub>Se<sub>3</sub>.

Sample	A <sub>1</sub> <sup>a</sup>	A <sub>2</sub> <sup>b</sup>	B <sub>1</sub> <sup>b</sup>	B <sub>2</sub> <sup>a</sup>
$\mu$ (cm <sup>2</sup> V <sup>-1</sup> s)	500	800	4500	3000
$T_F$ (K)	1150	900	87	100
$\frac{S^m}{T}$ ( $\mu\text{V K}^{-2}$ )	-0.4	-0.45	-6.1	-6.5
$\frac{\nu^m}{T}$ ( $\mu\text{V K}^{-2} \text{T}^{-1}$ )	0.009	0.012	1.24	2.4
$-\frac{\pi^2}{2} \frac{k_B}{e} \frac{1}{T_F}$	-0.2	-0.5	-4.9	-4.2
$283 \frac{\mu}{T}$ ( $\mu\text{V K}^{-2} \text{T}^{-1}$ )	0.009	0.02	1.44	0.86

<sup>a</sup>Measured down to 2 K.

<sup>b</sup>Measured down to 0.15 K.

measured (2K for A<sub>1</sub> and B<sub>2</sub> and 150 mK in the case of A<sub>2</sub> and B<sub>1</sub>), respectively. Values for the Fermi temperature and the mobility extracted from experiment were plugged in Eqs. (2) and (3). The expected values for the four samples are reported in the two last lines of Table I. The overall agreement between the measurement and the expected values is remarkable. This is particularly the case for the two samples studied at the lowest temperature (A<sub>2</sub> and B<sub>1</sub>).

### III. INVESTIGATION OF THE QUANTUM LIMIT OF THE BULK STATES OF Bi<sub>2</sub>Se<sub>3</sub>

When the carrier concentration becomes as low as  $10^{17} \text{ cm}^{-3}$ , the so-called *quantum limit* can be attained by a magnetic field of 15 T. In this limit all carriers are confined to their lowest Landau level. One essential parameter in this regime is the magnitude of the  $g$  factor. In the case of bismuth, for example, when the field is oriented along the trigonal direction, the  $g$  factor of the hole pocket is as large as 62. This corresponds to a ratio of the Zeeman energy ( $E_Z$ ) to the cyclotron energy ( $\hbar\omega_c$ ) labeled  $M = \frac{E_Z}{\hbar\omega_c}$  slightly larger than 2.<sup>21,22</sup> As a consequence, the chemical potential starts to move significantly with increasing magnetic field, dramatically affecting the Landau level spectrum.<sup>22</sup>

In the case of Bi<sub>2</sub>Se<sub>3</sub>, the data of sample B<sub>2</sub> down to  $T = 0.38$  mK and up to  $B = 17$  T does not reveal any Zeeman splitting of the peaks like the one found in bismuth.<sup>9,21</sup> This suggests that the Zeeman energy and the cyclotron energy are commensurate (i.e., that  $M$  is closed to an integer in the limit of the peak width) as originally suggested by Köhler *et al.*<sup>6</sup> In order to differentiate between  $M = 0, 1, 2, 3, \dots$ , we used a model similar to the one used by Köhler *et al.*<sup>6</sup> that determines the Landau level spectrum and the field dependence of the Fermi energy. The calculation of  $E_F$  is performed with the assumption that the carrier concentration (noted  $n$ ) is independent of the magnetic field (see Appendix A for a justification):  $n = \int_{-\infty}^{E_F} D(\epsilon) d\epsilon$  where  $D(\epsilon)$  is the density of state, equal to the sum of the density of state of each Landau level (noted LL) depending on their position relative to the Fermi energy (see Appendix C for more details).

#### A. $\alpha_{xy}$ or $N$ ?

One complication arises in comparing the experimental Nernst peaks and the theoretical Landau spectrum. Several theories were proposed to explain the observation of giant quantum oscillations in bismuth and graphite.<sup>11-13</sup> Two of these theories focus on the off-diagonal thermoelectric

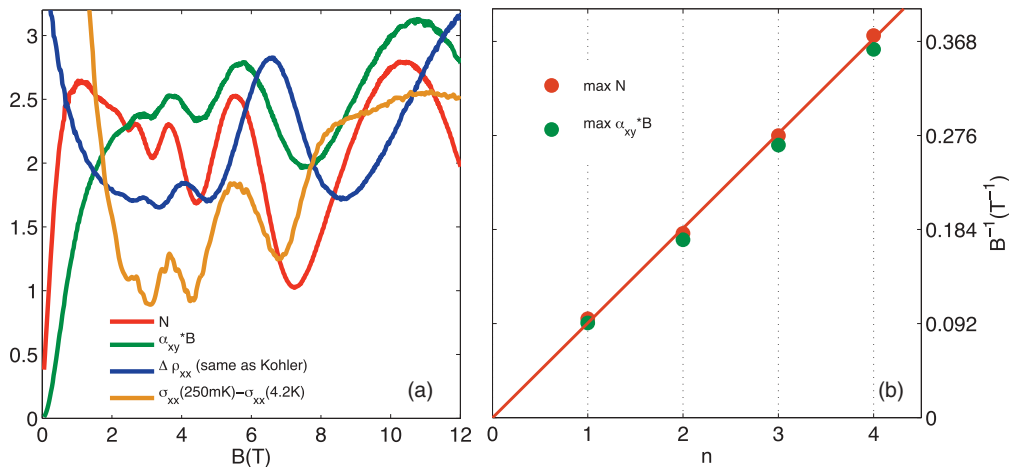


FIG. 5. (Color online) (a) Field dependence of the Nernst effect at  $T = 3$  K,  $\alpha_{xy} * B(T = 3 \text{ K})$ ,  $\Delta \rho_{xx}$  and  $\Delta \sigma_{xx} = \sigma_{xx}(0.25 \text{ K}) - \sigma_{xx}(4.2 \text{ K})$ , respectively, in red, green, blue, and dark orange. (b) Landau-level fan diagram for oscillations in  $N$  and  $\alpha_{xy} * B$ , respectively, red and green. The red line corresponds to a linear fit of the red points. As seen in (a), the peak positions in  $N$  and  $\alpha_{xy} * B$  are almost merging.

conductivity  $\alpha_{xy}$ ,<sup>11,12</sup> another one is based on a semiclassical description of the Nernst effect ( $N$ ).<sup>13</sup> In the case of bismuth and graphite, these two descriptions are equivalent because  $\rho_{xx} \gg \rho_{xy}$  and  $S \ll N$ . However, in the case of  $\text{Bi}_2\text{Se}_3$   $\rho_{xx}$  and  $\rho_{xy}$  become comparable in amplitude and therefore  $\alpha_{xy} * B$  and  $N$  do not peak exactly at the same magnetic field. We report in Fig. 5(a) the field dependence of the four quantities:  $\alpha_{xy} * B$ ,  $N$ ,  $\Delta \rho_{xx}$ , and  $\Delta \sigma_{xx} = \sigma_{xx}(0.25 \text{ K}) - \sigma_{xx}(4.2 \text{ K})$  (where  $\sigma_{xx} = \frac{\rho_{xx}}{\rho_{xx}^2 + \rho_{yy}^2}$ ) as a function of the magnetic field. Several conclusions can be drawn from this plot.

First,  $\alpha_{xy} * B$  and the Nernst effect do not peak exactly at the same magnetic field. Figure 5(b) shows the  $B^{-1}$  position of the Landau levels vs the index number. As seen in Fig. 5(a), the difference between the peak positions in  $\alpha_{xy} * B$  and in  $N$  is very small compared to the periodicity of the signals. Thus, our conclusions are not affected by the choice of  $\alpha_{xy} * B$  or the Nernst effect. Further theoretical investigations are needed to clarify this issue.

Second, the maxima of  $\Delta \sigma_{xx}$  are concomitant with the peak positions in  $\alpha_{xy}$  and the Nernst effect, whereas the maxima in  $\Delta \rho_{xx}$  are not. The origin of this difference is again related to the similar amplitudes of  $\rho_{xx}$  and  $\rho_{xy}$  above a few Tesla. Thus it appears that the enhancement of the conductivity generated by the crossing of an LL (Landau level) and the Fermi energy leads to a maximum in the Nernst response in the case of  $\text{Bi}_2\text{Se}_3$ , as it is the case for graphite and bismuth.

In Fig. 5(b) (Landau level fan), the intercepts of  $\alpha_{xy} * B$  and the Nernst effect are very close to 0, which is reminiscent of the nontrivial Berry phase as observed in  $\text{LaRhIn}_5$ .<sup>23</sup> In the case of  $\text{Bi}_2\text{Se}_3$ , which is characterized by a parabolic dispersion, the large spin orbit interaction generates this peculiar behavior. The occurrence of a vanishing intercept points out to an odd value for the ratio of the Zeeman energy and the cyclotron energy (labeled  $M$ ). This value is different from that deduced from the analysis of the peak position of  $\Delta \rho_{xx}$  by Köhler *et al.*<sup>6</sup> ( $M = 2$ ). However, as discussed previously, it has been shown that the peak position in  $\Delta \rho_{xx}$  differs from the Nernst response (and also differs from  $\sigma_{xx}$ ). In addition, as we approach the quantum limit, the spectrum analysis becomes more difficult

because of the field dependence of the Fermi energy. In order to clarify the possible values of  $M$  we proposed in the next section a detail analysis of the Nernst peaks using the simple model introduced in Appendix A.

### B. $g$ factor of the bulk states of $\text{Bi}_2\text{Se}_3$

The last peak resolved in the Nernst effect in sample  $\text{B}_1$  occurs at 10.4 T. We have adjusted the carrier concentration in order to find the best agreement between the position of this peak and the crossing points between a Landau level and the Fermi energy for different possible values of  $M$ . Figures 6(a)–6(d) show the Nernst effect (red lines) as a function of  $B^{-1}$ , superimposed with calculated Landau levels and Fermi energy  $E_F$  (black points) with various parameters:  $M = 0, 1, 2$ , and 3.

*a.  $M = 0$ .* In Fig. 6(a), we adjust the carrier concentration to match the periodicity of the Nernst response ( $n = 1.08 \times 10^{17} \text{ cm}^{-3}$ ). In this case, the crossings of the LL and the Fermi energy correspond to minima and not maxima. We cannot reproduce the lowest minimum of the Nernst effect. In Fig. 7(a), we try to adjust the carrier concentration to match the last resolved peaks at 10.4 T and the LL  $1^\pm$ . However, with this carrier concentration ( $n = 1.8 \times 10^{17} \text{ cm}^{-3}$ ), the low-field peaks cannot be reproduced at the right positions.

*b.  $M = 1$ .* Figure 6(b) shows the Landau level spectrum for a bulk carrier concentration of  $n = 1.28 \times 10^{17} \text{ cm}^{-3}$ . In this case, there is not a complete agreement for the two last peaks, but it is rather good for the other peaks. In the case of  $M = 1$ , the LL  $n + 1^-$  and  $n^+$  are degenerate except for the last ones:  $0^-$  [in orange on Fig. 6(b)]. The last observed peak at 10.4 T is attributed to the Landau levels  $0^+/1^-$ . Above this field all the electrons are in the lowest Landau level  $0^-$ .

*c.  $M = 2$ .* Figure 6(c) shows the Landau level spectrum for a bulk carrier concentration of  $n = 1.08 \times 10^{17} \text{ cm}^{-3}$ . We find a rather good agreement for all the peaks. Note that the agreement is slightly better for  $M = 2$  than for  $M = 1$ . In the case of  $M = 2$ , the LL  $n + 2^-$  and  $n^+$  are degenerate except for the two last ones  $1^-$  [in green on Fig. 6(c)] and  $0^-$  [in orange on Fig. 6(c)]. The last observed peak at 10.4 T

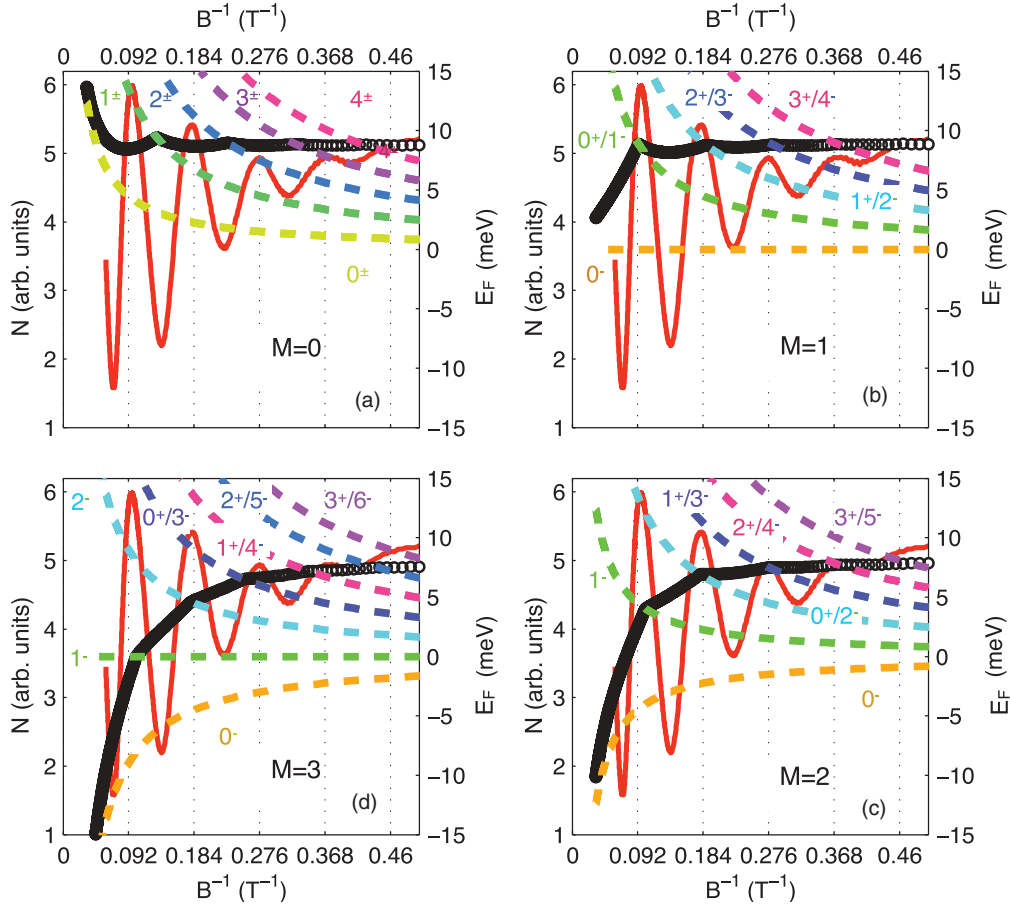


FIG. 6. (Color online) Nernst effect (red line) of the sample  $B_1$  at  $T = 3$  K on top of calculated Landau level energies and Fermi energy  $E_F$  (black open circle) with different parameters:  $M = 0, 1, 2$ , and  $3$  which, respectively, correspond to (a), (b), (c), and (d). The calculation was performed with a carrier concentration of  $n = 1.08 \times 10^{17} \text{ cm}^{-3}$  for (a), (b), and (d) and  $n = 1.25 \times 10^{17} \text{ cm}^{-3}$  for (b), a Dingle temperature of  $T_D = 8$  K and  $m_1 = m_2 = 0.14m_0$  and  $m_3 = 0.24m_0$ .

is then attributed to the Landau level  $1^-$  and the Landau levels  $n^-$  are degenerate with  $n-2^-$ . This result is compatible with the conclusion of the early Shubnikov-de Haas analysis.<sup>6</sup>

*d.  $M = 3$  (and above).* We also investigated higher values for  $M$ . On Fig. 6(d) ( $M = 3$ ), we report the Landau level spectrum for a carrier concentration of  $n = 1.08 \times 10^{17} \text{ cm}^{-3}$ . The lowest observed peaks match well the  $1^-$  LL. This result

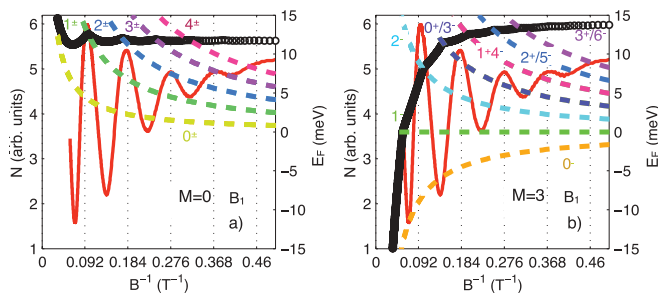


FIG. 7. (Color online)  $N$  (in red lines) of the sample  $B_1$  at  $T = 3$  K on top of a calculated Landau level energies and Fermi energy  $E_F$  (black open circle) with  $M = 0$  for (a) and  $M = 3$  for (b). In a case of (a) the carrier concentration has been chosen in order that the last resolved peak corresponds to the LL  $1^\pm$  ( $n = 1.8 \times 10^{17} \text{ cm}^{-3}$ ). For (b), the carrier concentration has been chosen in order that the last resolved peak matches the LL  $2^-$  ( $n = 2.9 \times 10^{17} \text{ cm}^{-3}$ ). The calculation was performed with a Dingle temperature  $T_D = 8$  K and  $m_1 = m_2 = 0.14m_0$  and  $m_3 = 0.24m_0$ .

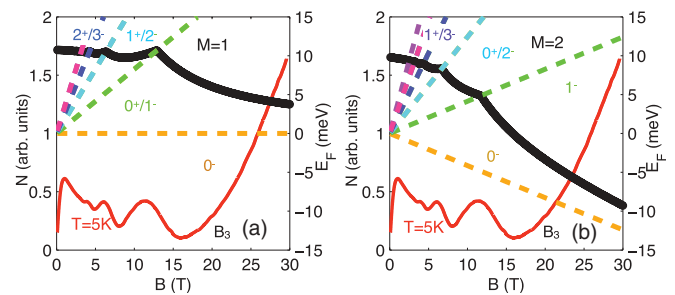


FIG. 8. (Color online) In red line is the Nernst effect,  $N$ , as a function of  $B^{-1}$  at  $T = 5$  K for the sample  $B_3$  (same as  $B_1$  few months after the (a) experiment) on (a) and (b). The evolution of the Fermi energy ( $E_F$ ) is plotted in black points. Each time that the chemical potential is crossing a Landau level (colors lines), there is a kink due to the carrier variation. The best parameter to describe the peak position as measured in  $N$  is found to be for  $M = 1$  (with a bulk carrier concentration  $n = 1.8 \times 10^{17} \text{ cm}^{-3}$ ) on (a) and  $M = 2$  (with a bulk carrier concentration  $n = 1.5 \times 10^{17} \text{ cm}^{-3}$ ) on (b).

is rather surprising as we would have naively expected that the field scale associated with the  $1^-$  LL would continuously increase with the value of  $M$ . In fact, even if the two lowest LL  $1^-$ ,  $0^-$  and the chemical potential are decreasing faster for  $M=3$  than for  $M=2$ , the crossing point between the LL  $1^-$  and the chemical potential occurs at the same field for  $M=2$  and  $M=3$ . This conclusion is true for all the values  $M > 2$ . The situation is, however, different for the other LL, where the crossing points differ for  $M=2$  and for  $M=3$ . In other words, for  $M=3$  we can find a carrier concentration where the 10.4 T peak matches the LL  $1^-$ , however, the peak positions at lower field cannot be explained. In Fig. 7(b), we investigate the possibility that the lowest observable peak is not associated with the  $1^-$  LL but with the  $2^-$  LL. We found a carrier concentration of  $n = 3 \times 10^{17} \text{ cm}^{-3}$ . However, the peak positions at lower fields cannot be explained.

In conclusion, the  $M=1$  and  $M=2$  hypothesis yields the best agreement between the peak positions in the Nernst effect and the crossing of Landau levels and the Fermi energy. Remarkably, in both cases above 10.4 T, all bulk carriers are spin polarized. For  $M=1$  and  $M=2$  and with a cyclotronic mass of  $0.14m_0$ , we find, respectively, that  $g = 14.3$  and  $g = 28.6$ .

### C. Nernst effect at high field

Sample  $B_3$  was studied up to 32 T. In this case, the last resolved peak in the Nernst effect occurs at 11.4 T because of a slightly higher carrier concentration. Interestingly, between 17 and 32 T, an unexpected increase of the Nernst effect was observed. At first glance, one could explain this increase by the presence of additional Landau levels which are expected in the case of  $M > 2$ . For instance, for  $M=3$ , the last observed peak could be attributed to the LL  $2^-$ . However, this scenario does not reproduce the low field peak positions. Moreover, it would yield a chemical potential crossing for the  $1^-$  LL at 19 T, in contrast with our experimental data.

The increase in the Nernst effect observed at high field calls for an alternative scenario. As reported in Fig. 8(b), once the  $1^-$  LL crosses the chemical potential, the enhanced shift in chemical potential pushes it closer towards the  $0^-$  LL. In the low field regime the Nernst response increases as the distance between the highest filled Landau level and the chemical potential becomes shorter and attains a maximum when the two levels coincide. Here if the chemical potential approaches the  $0^-$  LL without crossing it in order to keep charge neutrality, one expects it to peak without attaining a peak. This scenario can qualitatively explain the experimentally observed increase in the Nernst effect.

## IV. CONCLUSION

In conclusion, the overall thermoelectric and thermomagnetic response in  $\text{Bi}_2\text{Se}_3$  can be quantitatively understood in the context of a single three-dimensional band in the presence of large Zeeman splitting. Our investigation reveals a large variation of thermoelectric and thermomagnetic coefficients with the bulk carrier concentration which can be quantitatively understood as a result of a change in the mobility and the bulk Fermi energy. We resolved large quantum oscillations in the

Nernst coefficient suggesting that such an effect is a common feature to both compensated and noncompensated low carrier systems. For the lowest carrier concentrations investigated, we found that the Zeeman energy is either equal to one or two times the cyclotron energy. In both cases, a strong variation of the chemical potential above the quantum limit is expected, which can naturally explain the observed increase in the Nernst response. Finally we would like to point out that our results could impact the physics of the surface states. In the presence of a metallic bulk coupled with surface states, we can expect that the field-induced shift of the chemical potential of the bulk state could also generate a variation of the Fermi energy of the surface states. Such a situation will affect, for example, the Landau level indexing and the determination of the Berry phase of the surface state.

## ACKNOWLEDGMENTS

This work is supported by the Agence Nationale de Recherche as a part of the QUANTHERM project, by EuroMAGNET II under European Union Contract No. 228043. Work at Maryland was partially supported by the Lawrence Livermore National Laboratory LDRD program (Tracking Code 11-LW-003), operated under Department of Energy–National Nuclear Security Administration Contract No. DE-AC52-07NA27344.

## APPENDIX A: HALL EFFECT AND CARRIER CONCENTRATION

Figure 9 shows the field dependence of the Hall resistivity for five samples. Up to 32 T and down to the lowest carrier concentration investigated, the Hall effect was found to be linear in magnetic field suggesting that the carrier concentration remains constant and does not vary with the field. From the slope, we can determine the carrier concentration, labeled  $n^H$ . These values can be directly compared with the carrier concentration deduced from the period of the quantum oscillations labeled  $n^F$ . The conduction-band structure in this range of carrier densities is approximately parabolic. The Fermi energy is then determined by the period of the oscillation through the Onsager relation. Assuming a mass anisotropy independent of the doping ( $m_1 = m_2 = 0.14m_0$  and  $m_3 = 1.7m_1$ ) one can determine the carrier concentration of the samples. For all samples, within a few percent, we found a good agreement between  $n^F$  and  $n^H$ .

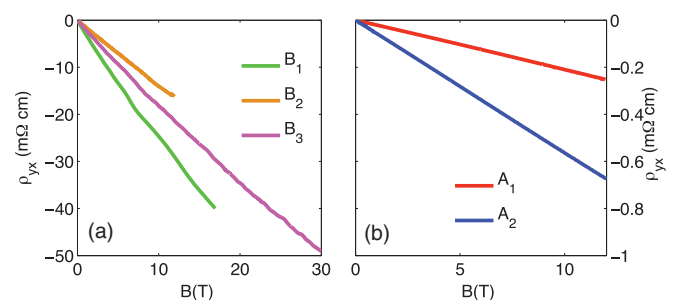


FIG. 9. (Color online) (a) Field dependence  $\rho_{yx}$  for  $B_1$  ( $T = 1.5$  K up to 12 T),  $B_2$  ( $T = 0.35$  K up to 17 T), and  $B_3$  ( $T = 1.6$  K up to 30 T). (b) Field dependence  $\rho_{yx}$  for  $A_1$  and  $A_2$  at  $T = 1.6$  K up to 12 T.

TABLE II. Comparison of the electronic mean free path and the distance between vacancy sites.

Sample	$n$ (cm <sup>-3</sup> )	$l_e$ (nm)	$d_v$ (nm)
A <sub>1</sub>	$3 \times 10^{19}$	23	2
B <sub>1</sub>	$2.5 \times 10^{17}$	550	10

### APPENDIX B: ELECTRONIC MEAN FREE PATH AND IMPURITY SCATTERING

In the case of Bi<sub>2</sub>Se<sub>3</sub> it is believed that Se vacancies are the charge dopants responsible for the  $n$ -type nature of the system. Here we propose to make a simple discussion to know if the vacancies are the main source of scattering of the electrons at low temperature. In other words we propose to compare the electronic mean free path and the distance between vacancies ( $d_v$ ). For the two extreme concentrations that we studied, we can determine the electronic mean free path  $l_e$  using the knowledge of the mobility and the Fermi velocity:  $l_e = v_F \tau = \frac{\hbar k_F \mu}{e}$ .

Each Se atom can contribute for two electrons. For a given bulk carrier concentration  $n$ , the number of lacuna per unit cell,  $N_i$  is given by  $N_i = \frac{nV}{2}$  where  $V$  is the unit volume. If we assume a homogeneous distribution of the lacuna, the typical distance between vacancies sites can be estimated:  $\frac{4}{3}\pi d_v^3 = \frac{V}{N_i} = \frac{1}{n}$ . Table II yields values of  $d_v$  for the two carrier concentrations. For both samples, the mean free path is longer than the typical distance between impurity sites, suggesting that the scattering probability between a traveling electron and a point defect is much smaller than unity.

### APPENDIX C: FIELD DEPENDENCE OF THE FERMI ENERGY

In the presence of a large  $g$  factor ( $M \geq 1$ ) for one single band, the Landau spectrum is modified in two ways:

(i) The quantum limit is reached at a higher magnetic field. For example, when  $M=2$ , the quantum limit is approximately one period above the quantum limit attained than in the case of  $M=0$ .

(ii) The lowest LL  $0^-$  is going down with increasing magnetic field. This pulls down the chemical potential near the quantum limit regime. In order to quantify these effects in the case of Bi<sub>2</sub>Se<sub>3</sub>, we compute the field dependence of the Fermi energy for various values of  $M$ . As discussed in Appendix A, we assumed that the carrier concentration is independent of the magnetic field and is given by  $n = \int_{-\infty}^{E_F} D(\epsilon) d\epsilon$  where  $D(\epsilon)$  is the density of state. In the presence of a magnetic field and in the absence of a spin splitting, the density of state  $D_0(\epsilon)$  can be written as

$$D_0(\epsilon) = \frac{\sqrt{m_0}}{2\pi^2 \hbar^2} eB \sum_{n=0}^{n_{\max}} \left[ \frac{\epsilon - \epsilon_n + \sqrt{(\epsilon - \epsilon_n)^2 + \Gamma^2}}{(\epsilon - \epsilon_n)^2 + \Gamma^2} \right]^{1/2} \times \begin{cases} 1 & \text{if } \epsilon > \hbar\omega_c/2 \\ 0 & \text{if } \epsilon < \hbar\omega_c/2, \end{cases} \quad (\text{C1})$$

where  $\epsilon_n = (n + \frac{1}{2})\hbar\omega_c$ ,  $n_{\max}$  is the highest value of  $n$  yielding a positive value for  $\epsilon - \epsilon_n$  and  $\Gamma$  is the broadening of the Landau levels ( $\Gamma = \pi \frac{k_B T_D}{e}$ ). In the presence of a spin splitting  $\epsilon_n = (n + \frac{1}{2} \pm \frac{M}{2})\hbar\omega_c$  where  $M = \frac{g m_c}{2m_0}$ . In this case, the density of state is given by  $D(\epsilon) = \frac{1}{2}(D_0(\epsilon - \frac{M}{2}\hbar\omega_c) + D_0(\epsilon + \frac{M}{2}\hbar\omega_c))$ .

\*benoit.fauque@espci.fr

†Present address: Condensed Matter and Materials Division, Lawrence Livermore National Laboratory, Livermore, CA 94550 USA.

<sup>1</sup>M. Z. Hasan and C. L. Kane, *Rev. Mod. Phys.* **82**, 3045 (2010).<sup>2</sup>G. S. Nolas, J. Sharp, and H. J. Goldsmid, *Thermoelectrics* (Springer, New York, 1962).<sup>3</sup>H. J. Goldsmid, *Proc. Phys. Soc. London* **71**, 633 (1958).<sup>4</sup>G. D. Mahan, *Solid State Phys.* **51**, 81 (1998).<sup>5</sup>N. P. Butch, K. Kirshenbaum, P. Syers, A. B. Sushkov, G. S. Jenkins, H. D. Drew, and J. Paglione, *Phys. Rev. B* **81**, 241301(R) (2010).<sup>6</sup>H. Köhler and E. Wüchner, *Phys. Stat. Sol.* **67**, 665 (1975).<sup>7</sup>Kazuma Eto, Zhi Ren, A. A. Taskin, Kouji Segawa, and Yoichi Ando, *Phys. Rev. B* **81**, 195309 (2010).<sup>8</sup>James G. Analytis, J. H. Chu, Y. Chen, F. Corredor, R. D. McDonald, Z. X. Shen, and I. R. Fisher, *Phys. Rev. B* **81**, 205407 (2010).<sup>9</sup>K. Behnia, M.-A. Méasson, and Y. Kopelevich, *Phys. Rev. Lett.* **98**, 166602 (2007).<sup>10</sup>Zengwei Zhu, Huan Yang, Benot Fauqu, Yakov Kopelevich, and Kamran Behnia, *Nat. Phys.* **6**, 26 (2010).<sup>11</sup>D. L. Bergman and V. Oganessian, *Phys. Rev. Lett.* **104**, 066601 (2010).<sup>12</sup>Y. V. Sharlai and G. P. Mikitik, *Phys. Rev. B* **83**, 085103 (2011).<sup>13</sup>Igor A. Luk'yanchuk, Andrei A. Varlamov, and Alexey V. Kavokin, *Phys. Rev. Lett.* **107**, 016601 (2011).<sup>14</sup>C. J. Bergeron, C. G. Grenier, and J. M. Reynolds, *Phys. Rev. Lett.* **2**, 40 (1959).<sup>15</sup>R. Fletcher, *Phys. Rev. B* **28**, 6670 (1983).<sup>16</sup>M. M. Gadzhialiev, *Sov. Phys. Semicon.* **2**, 833 (1969).<sup>17</sup>B. Tieke, R. Fletcher, J. C. Maan, W. Dobrowolski, A. Mycielski, and A. Wittlin, *Phys. Rev. B* **54**, 10565 (1996).<sup>18</sup>D. Shoenberg, *Magnetic Oscillations in Metals* (Cambridge University Press, Cambridge, 1984).<sup>19</sup>K. Behnia, *J. Phys.: Condens. Matter* **21**, 113101 (2009).<sup>20</sup>K. Behnia, D. Jaccard, and J. Flouquet, *J. Phys.: Condens. Matter* **16**, 5187 (2004).<sup>21</sup>S. G. Bompadre, C. Biagini, D. Maslov, and A. F. Hebard, *Phys. Rev. B* **64**, 073103 (2001).<sup>22</sup>Zengwei Zhu, Benot Fauqué, Yuki Fuseya, and Kamran Behnia, *Phys. Rev. B* **84**, 115137 (2011).<sup>23</sup>G. P. Mikitik and Yu. V. Sharlai, *Phys. Rev. Lett.* **93**, 106403 (2004).